Discrete Functional Gold Nanoparticles: Hydrogen Bond-Assisted Synthesis, Magnetic Purification, Supramolecular Dimer and Trimer Formation

Chun-Pong Chak,[†] Shouhu Xuan,[†] Paula M. Mendes,[‡] Jimmy C. Yu,[†] Christopher H. K. Cheng,[§] and Ken Cham-Fai Leung[†,*]

[†]Center of Novel Functional Molecules, Department of Chemistry, The Chinese University of Hong Kong, Shatin, NT, Hong Kong, [‡]College of Engineering and Physical Sciences, School of Chemical Engineering, The University of Birmingham, Edgbaston, Birmingham B15 2TT, United Kingdom, and [§]Department of Biochemistry (Medicine), The Chinese University of Hong Kong, Shatin, NT, Hong Kong

ABSTRACT Amine monofunctional gold nanoparticles (1-AuNPs) were synthesized by employing a solid-supported technique and pH-switchable pseudorotaxane formation. Purification was repeatedly facilitated using crown ether peripherally coated superparamagnetic iron oxide microspheres to yield the monofunctional gold nanoparticles in excellent yield. The product and its related intermediate superstructures were characterized by IR and X-ray photoelectron spectroscopies. Novel supramolecular dimers and trimers were prepared by titrating the 1-AuNPs with bisDB24C8 and trisDB24C8 at different ratios. UV/visible absorption spectroscopic analyses of the supramolecular dimer and trimer solutions, which were formed by mixing their separate components in different ratios, indicated the gradual appearance of two distinct plasmonic resonance bands at 620 and ~700 nm. Furthermore, TEM images of the dimers revealed a significant amount of dimer pairs on the surface, while the TEM images of the trimers demonstrated the presence of both dimers and trimers. The trimers appeared as triangular or near-linear shapes.

KEYWORDS: amine · gold · iron oxide · nanoparticle · supramolecular

Nanoparticles (NPs) are powerful tools for *in vitro* and *in vivo* diagnostic, imaging, immunolabeling, and therapy due to their biomimetic features, their high surface area to volume ratio, and the possibility of modulating their surface properties with biomolecules.[1−3] The potential of nanoparticles in biology and medicine has just begun to be realized, and new avenues will be opened as our ability to manipulate these materials improves.[4,5] Significant advances have been made over the past decade in the wet-chemical syntheses of robust single-component NPs in a wide range of sizes, shapes, and protective organic layers. Typically, the composition of functional groups in the NPs can be varied through ligand exchange by using different capping-ligand mixtures.[6] However, with such approaches, it is rather difficult to prepare nanoparticles with a discrete number of chemical functional groups. By way of an example, alkanethiol-coated gold NPs[7−13] can be functionalized by place exchange reactions with different types of thiolate ligands having designed terminal reactive end groups. However, such displacement reactions produce randomly functionalized NPs so that the number of newly displaced, reactive ligands is uncertain and may vary from NP to NP. To date, examples have been reported wherein monofunctionalized nanoparticles have been prepared.[14−28] For instance, Worden *et al.*[14] and Sung *et al.*[15] developed solid-phase chemistry methods to prepare gold nanoparticles with single functional groups. These methodologies relied on the covalent bonding of a bifunctional ligand (*e.g.*, thiol and carboxylic acid groups) onto a Wang resin solid support and the subsequent one-to-one place exchange reaction between the support-bound thiol ligands and the gold nanoparticles. After cleaving off from the solid support, monofunctionalized nanoparticles were obtained. However, the described methods[14,15] showed low percentage yields of the resulting monofunctionalized NPs that are associated with several covalent bond-forming/breaking reactions. Other limitations include long reaction times and harsh reaction conditions. In the latest concept developed by Krüger *et al.*,[16] gold nanoparticles were functionalized with single carboxyl groups using nanoparticle surface polymerization. This methodology may provide better yields, but it lacks flexibility on the physical properties of the

*Address correspondence to cfleung@cuhk.edu.hk.

Received for review March 31, 2009 and accepted July 15, 2009.

Published online July 21, 2009.
10.1021/nn9005895 CCC: $40.75

nanoparticle surface coating. Thus, there is a pressing need to develop effective strategies for functionalizing and purifying nanoparticles with a controlled number of chemical functional groups.

Research in supramolecular chemistry has progressed from the investigations of the basis of molecular recognition to the construction of novel functional molecules, including molecular switches, molecular motors, artificial molecular muscles, and molecular elevators.[29,30] Furthermore, besides the design of novel organic supramolecular architectures, recent years have witnessed the application of supramolecular concepts to the development of organic−inorganic hybrid materials[31] with improved functionalities. For instance, heterosupramolecular approaches have provided a means of enhancing recognition and sensing on surface materials, of building reversible nanometer-sized networks and 3D architectures, as well as of incorporating biomimetic and gated chemistry in hybrid nanomaterials.[32] Recent examples demonstrate that the combination of supramolecular principles and inorganic nanomaterials can lead to the fine-tuning of material properties, opening new perspectives for the application of supramolecular concepts.

Armed with this background, we report herein a method to functionalize gold NPs (2 nm) specifically with an amine group employing a solid-supported technique using pH-switchable supramolecular recognition motifs[33,34] and nanoparticle-based magnetic separation.[35,36] Supramolecular recognition motifs involving dibenzo[24]crown-8 (DB24C8) and dibenzylammonium (DBA), which form a 1:1 supramolecular complex, namely, [DBA⊂DB24C8] pseudorotaxane,[37−39] were selected for this study because of their capability to function as pH-switchable templates. The pseudorotaxane, which is ON/OFF switchable upon pH changes, is stabilized principally by [C−O···H−N^+] and [C−O···H−C−N^+] hydrogen bonds with additional secondary stabilization coming from electrostatic and π−π interactions. Multivalent assemblies between the molecular recognition motifs to form pseudorotaxanes are feasible *via* a self-sorting process. Magnetic separation is based on superparamagnetic iron oxide (SPIO) NPs[40] that are decorated with DB24C8 at the peripheries. The DB24C8-functionalized SPIO NPs can be used to harness all amine/ammonium-functionalized gold NPs out of the reaction mixture by an externally applied magnetic field. By employing these supramolecular materials as well as the magnetic recycling purification processes, the yields in affording the discretely functionalized gold NPs will be greatly enhanced since most of the low-yielding processes involving the covalent bond-forming and -breaking reactions are eliminated. Moreover, the solid-phase supports and the magnetic particles are recyclable and reusable, rendering them as versatile tools for the synthesis and purification of this type of demanding NPs. In contrast, typical chromatographic separation and purification of products often require a large amount of solvents and are time-consuming. Characterization of the discrete functional gold NPs by infrared (IR), UV/visible absorption, and X-ray photoelectron spectroscopies and transmission electron microscopy (TEM) confirms the formation of amine monofunctional gold nanoparticles in near-quantitative yield.

RESULTS AND DISCUSSION

To begin with, DB24C8-CO_2H[41] was treated (Figure 1) with isobutylchloroformate (IBCF) to form an anhydride *in situ* prior to the addition of polystyrene (PS) resin (PS Wang resin, poly(4-(4-vinylbenzyloxy)benzyl alcohol), hydroxyl group functional density = 1.0−1.5 mmol/g) to give the DB24C8-decorated resin (PS-DB24C8) in 77% yield. Then, the PS-DB24C8 was swelled in a CH_2Cl_2/MeCN (6:1) mixture followed by the self-assembly[42,43] with the DBA−disulfide ligand **1** · HPF_6[44] to yield the PS-DB24C8⊃[**1** · HPF_6]$_n$. Subsequently, a slight excess of gold NPs (AuNPs, 2 nm) was added to the poly(pseudorotaxane) structure PS-DB24C8⊃[**1** · HPF_6]$_n$. This process resulted in the disulfide place exchange reaction between the disulfide ligands **1** · HPF_6 and butyl thiolates, leading to the immobilization of AuNPs to form the PS-DB24C8⊃[**1** · HPF_6-AuNP]$_n$. Accounting to the site isolation effect from which the DB24C8 groups on PS were not in close proximity, each self-assembled disulfide ligand most likely reacted with only one AuNP. Finally, the PS-DB24C8⊃[**1** · HPF_6-AuNP]$_n$ structure was incubated with a solution of Et_3N in CH_2Cl_2 for the deprotonation of all ammonium ions into amines. As a result, the crown ether had lost its hydrogen-bonded binding affinity toward the amine ligand, from which the AuNPs bearing the amine ligand (**1**-AuNPs) were separated out from the solid PS-DB24C8. Clearly, the product that was isolated after the final deprotonation step not only contained the 1-AuNPs but also might contain the unreacted, physisorbed AuNPs, the unreacted deprotonated ligand **1**, and any AuNP with more than one ligand attached to it (**1**$_n$-AuNPs). Thus, an effective and efficient purification method must be provided for the complete isolation of the **1**-AuNPs.

A purification procedure for the crude **1**-AuNP mixture was designed (Figure 2) and facilitated using the DB24C8-functionalized silica-coated SPIO microspheres (SPIO−DB24C8, size ∼200 nm). The SPIO−DB24C8 microspheres are composed of ∼6 nm SPIO crystals confined in thin silica shells, which are decorated with the crown ethers by amide linkages.[45] These magnetic microspheres are compatible with a dilute acid (*i.e.*, trifluoroacetic acid, H-TFA) and a dilute base (*i.e.*, Et_3N). Fortunately, we found out that the amine ligand **1** in the mixture could be effectively washed away using EtOH at 0 °C without jeopardizing other AuNP-related structures. Subsequently, the resulting ligand-free mix-

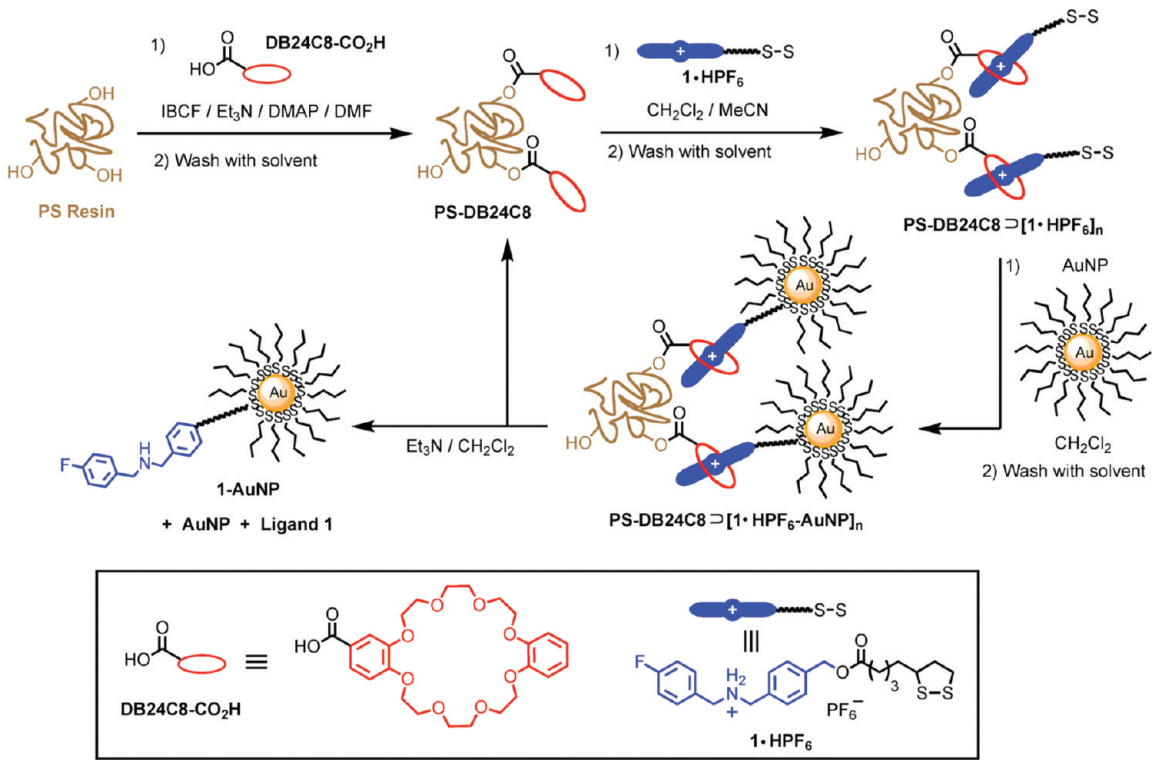

Figure 1. Graphical representation of the solid-supported preparation of monofunctional gold nanoparticles, featuring supramolecular recognition motifs in the form of dibenzo[24]crown-8 (DB24C8) on polystyrene (PS) resin and dibenzyl ammonium (DBA)−disulfide ligand.

ture was treated with H-TFA and the SPIO−DB24C8. The protonated **1** · HTFA-AuNPs were captured by the SPIO−DB24C8 microspheres, which were subsequently attracted by an externally applied magnetic field. The unreacted excess of AuNPs, which were not self-assembled on the SPIO−DB24C8 microspheres, were washed away. While the magnetic field was still being applied to the **1** · HTFA-AuNPs-functionalized SPIO−DB24C8 microspheres, the microspheres were subjected to a base treatment with Et_3N for the deprotonation of all ammonium ions, releasing the purified **1**-AuNPs. The SPIO−DB24C8 microspheres were reused for repeated purification cycles. We found out experimentally that complete isolation of the **1**-AuNPs can be obtained after repeating the purification process 5−7 times using the SPIO−DB24C8 microphores. The overall conversion yields are 3.0 mg of **1**-AuNP per gram of PS resin (−OH density = 1.0−1.5 mmol/g) and 2.3 mg

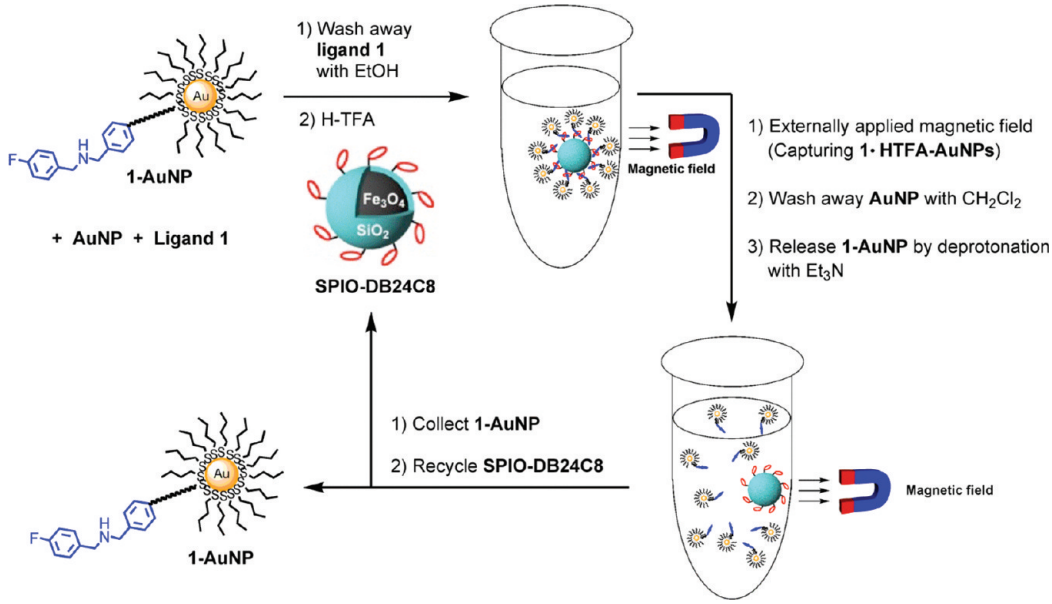

Figure 2. Graphical representation of the magnetic purification process for the 1-AuNPs from the crude mixture.

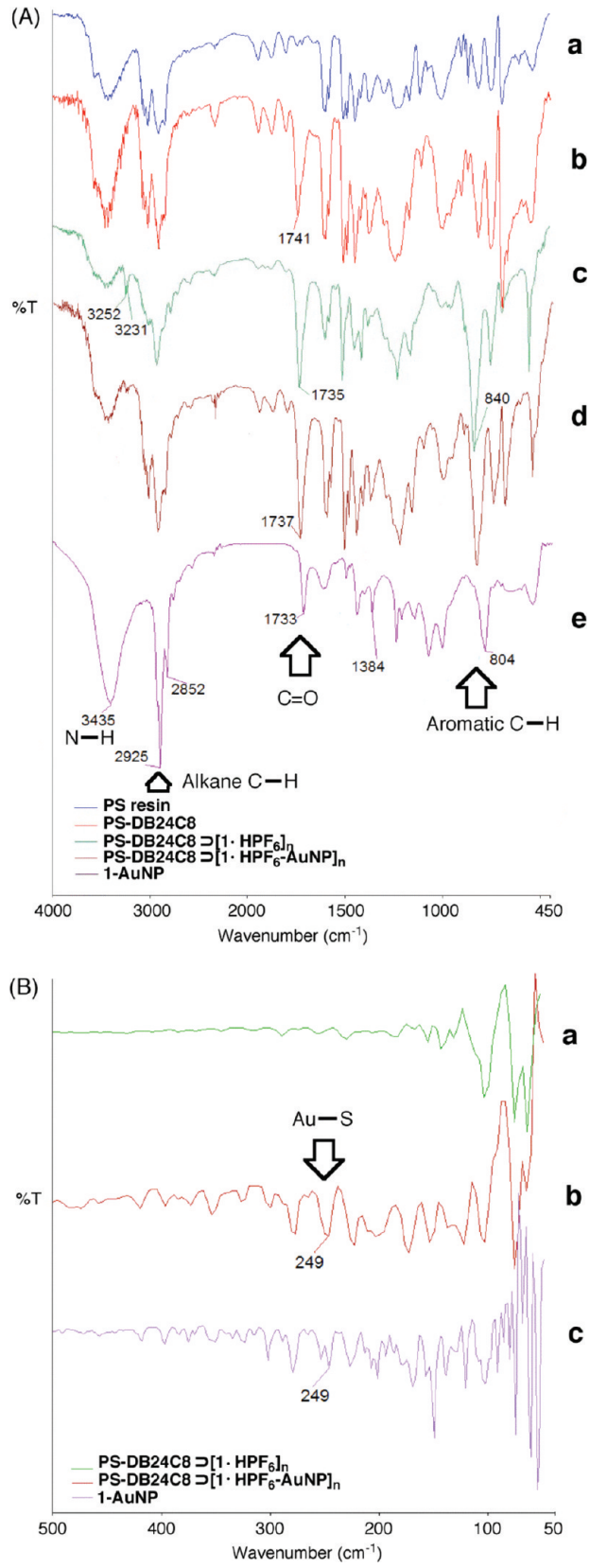

Figure 3. (A) Stacked FTIR absorption spectra of (a) PS resin, (b) PS-DB24C8, (c) PS-DB24C8⊃[1 · HPF_6]$_n$, (d) PS-DB24C8⊃[1 · HPF_6-AuNP]$_n$, and (e) 1-AuNP. (B) Stacked far-IR absorption spectra of (a) PS-DB24C8⊃[1 · HPF_6]$_n$, (b) PS-DB24C8⊃[1 · HPF_6-AuNP]$_n$, and (c) 1-AuNP.

of **1**-AuNP per gram of PS-DB24C8 (−DB24C8 density ~ 1.0 mmol/g). The yield is near quantitative after several repeated purification steps.

The characterization of the step-by-step intermediate structures was monitored by FTIR, far-IR (Figure 3 and Table S1 in Supporting Information), and XPS spectroscopies (Figures S9−S13 in Supporting Information). From the FTIR spectrum of the PS resin, three main IR absorptions are observed and assigned (Figure 3A,a).[46] They are O−H stretching (~3400 cm^{-1}), alkane C−H stretching (2920 and 2960 cm^{-1}), and aromatic absorptions (~1600, 1200−1500, and ~900), which reveal the presence of hydroxyl groups, PS alkane backbone, and benzyl aromatic rings, respectively. For the FTIR spectrum of the PS-DB24C8 (Figure 3A,b),[47] the absorption bands are similar to those of the PS resin except for the appearance of a sharp carbonyl absorption at 1741 cm^{-1}, which originates from the ester linkage after the condensation reaction between the PS resin and DB24C8-CO_2H. When the ligand **1** · HPF_6 was treated with the PS-DB24C8 followed by a washing process, the remaining solid gave (Figure 3A,c) two new sets of IR modes at ~3230−3260 cm^{-1} (N^+−H stretching) and 840 cm^{-1} (*para*-substituted aromatic C−H). Moreover, the percentage transmission (%T) of the carbonyl absorption at 1735 cm^{-1} increased, revealing the successful self-assembly of the ester-containing ligand **1** · HPF_6 onto the PS-DB24C8 to form the poly(pseudorotaxane) PS-DB24C8⊃[**1** · HPF_6]$_n$. After the subsequent addition of AuNPs followed by a washing step, the remaining solid gave similar FTIR absorption bands (Figure 3A,d) to those found in the PS-DB24C8⊃[**1** · HPF_6]$_n$ (Figure 3A,c). However, by comparing the far-IR spectrum of the PS-DB24C8⊃[**1** · HPF_6]$_n$ (Figure 3B,a) with that of the remaining solid (Figure 3B,b), a new absorption band at 249 cm^{-1} and other new weak bands were identified that correspond to the Au−S absorption.[48,49] Thus, the observation of these new bands demonstrates the successful immobilization of the AuNPs onto the PS-DB24C8⊃[**1** · HPF_6]$_n$ structure to form the PS-DB24C8⊃[**1** · HPF_6-AuNP]$_n$. Following the magnetic purification steps, the **1**-AuNPs were also characterized by both FTIR and far-IR spectroscopies. Major absorption bands were observed (Figures 3A,e,B,c) at ~3400 cm^{-1} (N−H stretching), 2852 and 2925 cm^{-1} (alkane C−H stretching), 1733 cm^{-1} (C═O absorption), 1600 cm^{-1} (aromatic overtone), 1384 cm^{-1} (CH_3 symmetrical deformation, from the *n*-butylthiolate ligands), 804 cm^{-1} (*para*-substituted aromatic C−H), and 249 and 250 cm^{-1} (Au−S absorption). The absorption bands, which are assigned to the C−H asymmetric and symmetric methylene stretching vibration, are shifted to lower wavenumbers from 2920 to 2852 cm^{-1} and from 2960 to 2925 cm^{-1}.[50] Among these observed major IR absorption bands, the secondary amine (R_2N−H) bending, the secondary ammonium (R_2N^+−H) stretching, C−S and S−S absorption bands are too weak to be ob-

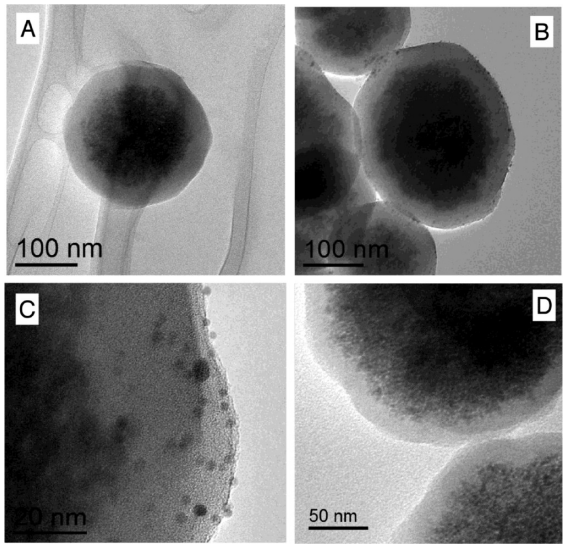

Figure 4. TEM images of (A) SPIO−DB24C8 microsphere; (B,C) SPIO−DB24C8⊃[1 · HTFA-AuNP]$_n$; and (D) remaining SPIO−DB24C8 microspheres after base treatment of the SPIO−DB24C8⊃[1 · HTFA-AuNP]$_n$.

served. Furthermore, the characterization of the intermediate nanostructures (*i.e.*, SPIO-NH_2, SPIO−DB24C8, and SPIO−DB24C8⊃[**1** · HTFA-AuNP]$_n$) was also monitored by FTIR spectroscopy (Figure S8 in Supporting Information).

XPS spectra were also acquired for the PS resin, PS-DB24C8, PS-DB24C8⊃[**1** · HPF_6]$_n$, PS-DB24C8⊃[**1** · HPF_6-AuNP]$_n$, and **1**-AuNP samples (Figures S9−S13 in Supporting Information). As expected, XPS analyses of the PS resin and PS-DB24C8 showed (Figures S9 and S10 in Supporting Information) the presence of carbon and oxygen. However, XPS spectrum of the PS-DB24C8⊃[**1** · HPF_6]$_n$ revealed (Figure S11 in Supporting Information) additional peaks at 685 eV (F 1s), 400 eV (N 1s), and 162 eV (S 2p), which demonstrate the successful self-assembly of the DBA−disulfide ligand **1** · HPF_6 onto the PS-DB24C8 to form the PS-DB24C8⊃[**1** · HPF_6]$_n$. In addition to these peaks, XPS spectra of the PS-DB24C8⊃[**1** · HPF_6-AuNP]$_n$ (Figure S12 in Supporting Information) and **1**-AuNP (Figure S13 in Supporting Information) exhibited the characteristic Au $4f_{5/2}$ (86 eV) and Au$4f_{7/2}$ (83 eV) peaks, confirming that AuNPs were immobilized on the PS-DB24C8⊃[**1** · HPF_6]$_n$ to form the PS-DB24C8⊃[**1** · HPF_6-AuNP]$_n$ and then released to form the **1**-AuNPs.

TEM was employed for the structural characterization of the nanostructures obtained at the different magnetic purification steps (Figure 4). Figure 4A reveals the morphology of a typical SPIO−DB24C8 microsphere with a diameter of 220 nm. The SPIO−DB24C8 microspheres were used to abstract all the functionalized AuNPs by forming the hydrogen-bonded supramolecular pseudorotaxane structures in a multivalent manner. The nanostructures SPIO−DB24C8⊃[**1** · HTFA-AuNP]$_n$ were characterized by TEM (Figure 4B,C). It is clearly observed that smaller AuNPs (2 nm) are well deposited on the periphery of the SPIO−DB24C8 microspheres. Energy dispersive X-ray (EDX) spectroscopy was performed for the elemental analysis of SPIO−DB24C8⊃[**1** · HTFA-AuNP]$_n$ that showed the presence of Au, Fe, C, O, Si, and Cu (Figure S7b in Supporting Information). The presence of Au in the EDX spectrum of SPIO−DB24C8⊃[**1** · HTFA-AuNP]$_n$, which is different from the EDX spectra of SPIO−DB24C8 before (Figure S7a in Supporting Information) and after (Figure S7c in Supporting Information) base treatment, indicates the successful self-assembly and isolation of the functionalized AuNPs from the crude mixture. Furthermore, Figure 4D shows the TEM image of the SPIO−DB24C8 microspheres after treatment of SPIO−DB24C8⊃[**1** · HTFA-AuNP]$_n$ with a base and subsequent isolation of the purified **1**-AuNPs. In particular, small AuNPs were not observed at the periphery of the

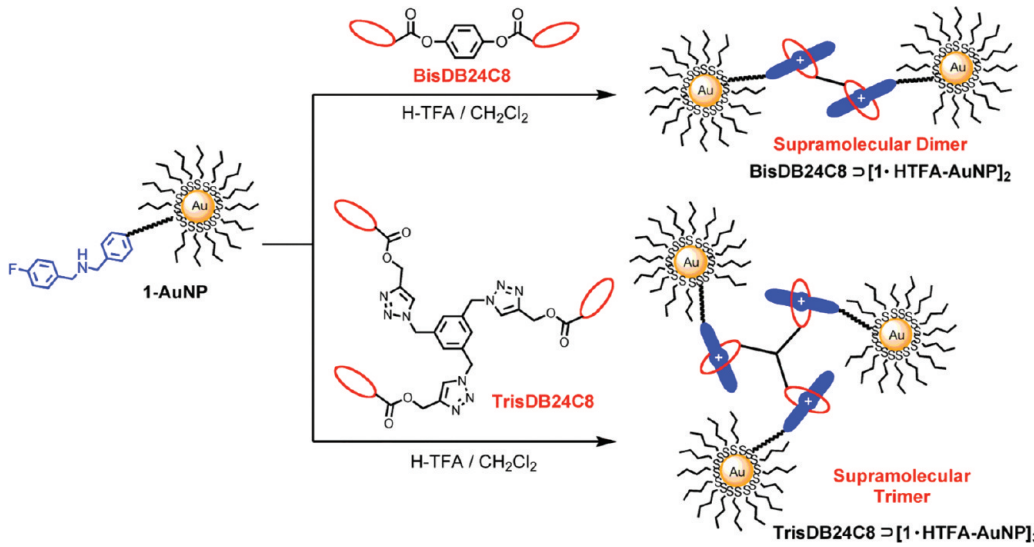

Figure 5. Supramolecular self-assembly of the 1-AuNPs with bisDB24C8 and trisDB24C8 to afford the dimers bisDB24C8⊃[1 · HTFA-AuNP]$_2$ and trimers trisDB24C8⊃[1 · HTFA-AuNP]$_3$, respectively.

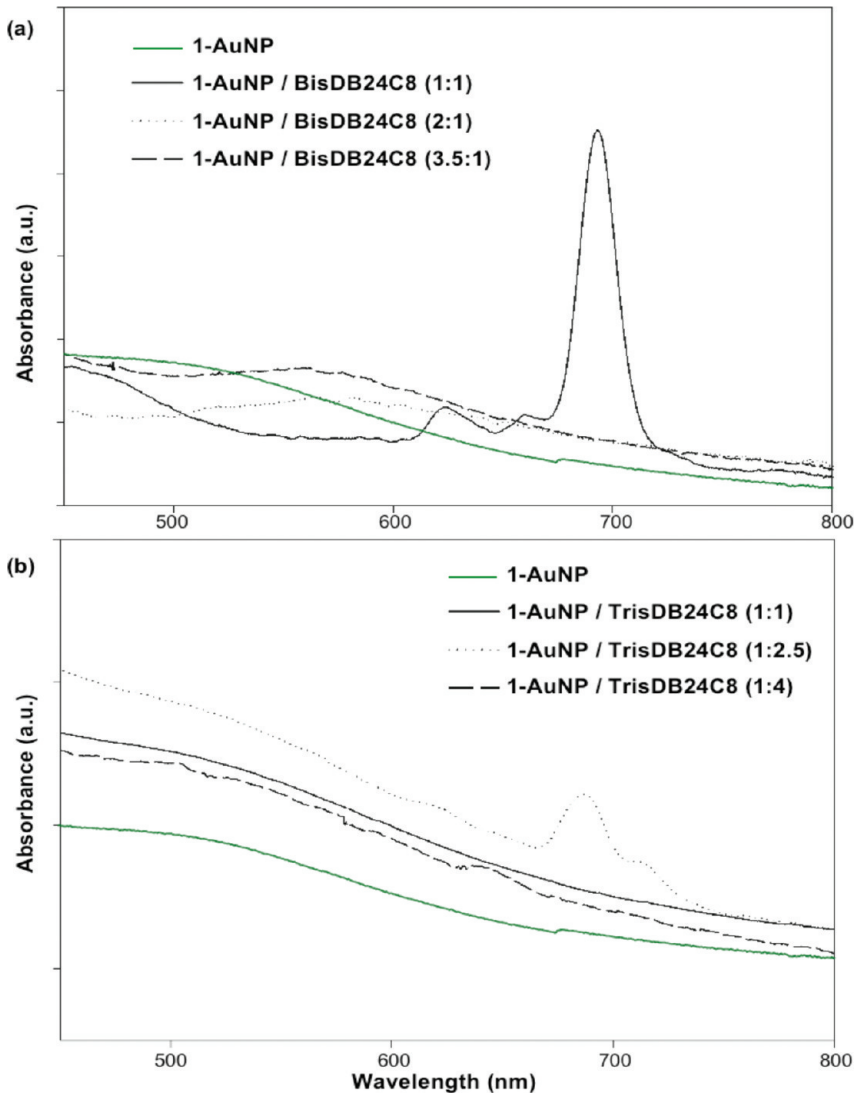

Figure 6. Stacked UV/visible absorption spectra (CH_2Cl_2, 298 K) of (a) 1-AuNP titrated with different amounts of bisDB24C8 (w/w = 1:1, 2:1, and 3.5:1) and (b) 1-AuNP titrated with different amounts of trisDB24C8 (w/w = 1:1, 1:2.5, and 1:4).

SPIO−DB24C8 microspheres, a result that indicates an effective and complete isolation of the purified **1**-AuNPs using the pH-switchable, hydrogen-bonded molecular recognition units.

It is assumed that, when the purified monofunctional 1-AuNPs are treated with divalent linkers, dimers will form. The characterization of these dimers is feasible by UV/visible spectroscopy and TEM inspection. Herein, the pH-switchable supramolecular motifs have been exploited (Figure 5) to form supramolecular dimers and trimers by virtue of the self-assembly using bisDB24C8 and trisDB24C8 compounds. Briefly, the bisDB24C8 was synthesized *via* a divalent condensation reaction between DB24C8-CO_2H and hydroquinone, while the trifurcated trisDB24C8 was synthesized *via* a 1,3-dipolar cycloaddition reaction—"click" chemistry approach[51,52] with high efficiencies between the DB24C8-$CO_2CH_2C{\equiv}CH$ and 1,3,5-tris(azidomethyl)benzene. The purified **1**-AuNPs were first protonated by H-TFA in CH_2Cl_2 and then mixed with either the bisDB24C8 or trisDB24C8 to afford the corresponding supramolecular dimers bisDB24C8⊃[**1** · HTFA-AuNP]$_2$ or the supramolecular trimers trisDB24C8⊃[**1** · HTFA-AuNP]$_3$.

The obtained AuNP structures including their dimers and trimers were investigated by UV/visible absorption spectroscopy (Figure 6). The 2 nm butylated AuNP demonstrated the well-known plasmonic band at $\lambda \sim 520$ nm,[17,49,53,54] while the monofunctional **1**-AuNP revealed the same plasmonic absorption at $\lambda \sim 520$ nm as well as a shoulder peak at $\lambda \sim 260$ nm, originating from the aromatic absorption of the attached ligand (Figure S5 in Supporting Information).

Since it is a difficult task to measure the amounts of the bisDB24C8 and trisDB24C8 in exact stoichiometric ratios for the self-assembly with **1**-AuNP, it is necessary to perform several titration experiments by mixing the purified **1** · HTFA-AuNPs with the linkers in different ratios (w/w). In particular, a series of supramolecular species was obtained by mixing the purified **1** · HTFA-AuNPs with bisDB24C8 in CH_2Cl_2 in different ratios: 1:1, 2:1, and 3.5:1 (w/w). After the addition of bisDB24C8 linker and **1**-AuNP in a ratio of 1:1 (w/w), the absorption increased in intensity and completely red-shifted to ~700 and 620 nm (Figure 6a).[53] The appearance of the sharp plasmonic absorption band at ~700 nm indicates the formation of **AuNP** aggregates where the **AuNPs** are in close proximity. When the amounts of the **1-AuNP** increase in the solutions (w/w = 2:1 and 3.5:1), the plasmonic absorption band at ~700 nm disappeared but with the observation of new red-shifted local absorption maxima at ~580 nm. These results suggest that modest amounts of AuNP aggregate are still present in these mixtures.

Similarly, the **1**-AuNPs were titrated with the trisDB24C8 linker in different ratios (w/w = 1:1, 1:2.5, and 1:4). A sharp plasmonic absorption at ~700 nm indicates AuNP aggregation was observed for the ratio of 1:2.5 between **1**-AuNP and trisDB24C8 (Figure 6b). The intensity of this plasmonic absorption, however, is not as strong as that observed using the bisDB24C8. Additions of base into the solutions, which contain the supramolecular species, disrupt the self-assemblies. The UV/visible spectrum of the resulting solution is simply

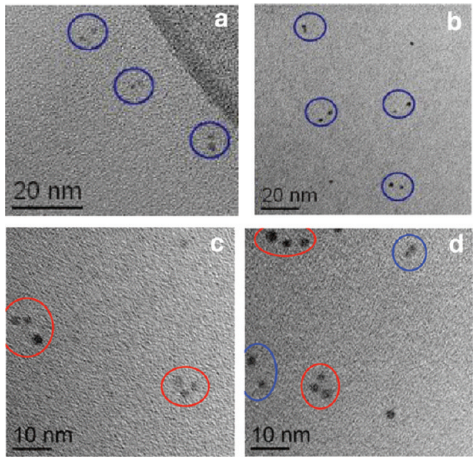

Figure 7. Transmission electron microscopic images of (a,b) the supramolecular dimers prepared by mixing 1-AuNPs ([1-AuNP] ~ 0.2 mg/mL) with bisDB24C8 in the ratio of 1:1 w/w, and (c,d) the supramolecular trimers prepared by mixing 1-AuNPs ([1-AuNP] ~ 0.2 mg/mL) with trisDB24C8 in the ratio of 1:2.5 w/w. Note the blue circles indicate the dimers, and the red circles indicate the trimers.

the sum of their UV/visible spectra of separate components. Consequently, these observations prove the successful self-assembly between the **1**-AuNPs and the linkers as the form of supramolecular species. Furthermore, the actual structural identities of these supramolecular species could be revealed by immobilizing them on a surface and observing the surface under TEM.

A control experiment has been performed in the absence of the PS-DB24C8 resin. Therefore, the AuNPs were randomly functionalized with ligand **1** by means of an uncontrolled place exchange reaction. When these randomly ligand-functionalized AuNPs were treated with different amounts the bisDB24C8, 3D network scaffolds were formed (Figure S14 in Supporting Information) and revealed maximum plasmon bands at 620 and 700 nm (Figure S15 in Supporting Information). Another control experiment has been performed by treating the **1**-AuNPs with DB24C8 (instead of bisDB24C8) and HTFA. The DB24C8 macrocycle self-assembles with **1** · HTFA-AuNPs to yield the supramolecular complex DB24C8⊃[**1** · HTFA-AuNP]. The resulting mixture was analyzed by TEM, which reveals an image with segregated nanoparticles (Figure S16b in Supporting Information).

The titrated solutions, which contain the supramolecular species, were analyzed by TEM. For the solution of **1**-AuNP/bisDB24C8 (w/w = 1:1) as revealed by TEM analysis (Figure 7a,b), significant amounts of dimer pairs are observed. The apparent spacing between two AuNPs in the dimer structures ranges from 2.8 to 4.7 nm (Figures S18−S20 in Supporting Information). Among other solutions with different titration ratios, the TEM images of the solution w/w = 1:1 yield higher number of dimers (Figure S17a in Supporting Information). No higher order supramolecular structures (trimers, tetramer, *etc.*) are observed under TEM (Figure 8a).

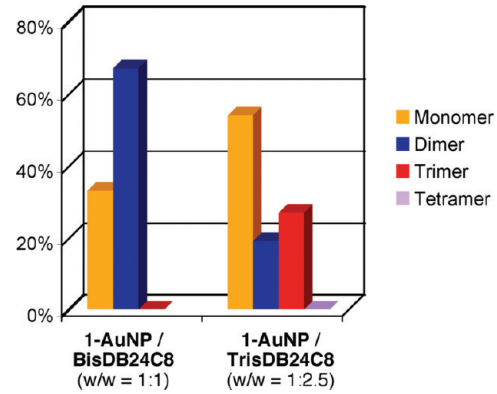

Figure 8. Statistical distributions in TEM analysis of the solution (a) 1-AuNP/bisDB24C8 (w/w = 1:1) and (b) 1-AuNP/trisDB24C8 (w/w = 1:2.5). Spectra with approximately 100 particles were analyzed.

Therefore, the obtained product did not contain any multifunctional AuNPs (difunctional, trifunctional, *etc.*, $\mathbf{1}_n$-AuNPs) but only monofunctional **1**-AuNPs in near-quantitative yield. It is a fact that the supramolecular species are concentration-dependent. Thus, the observation of individual NPs in the mixture, which was analyzed by TEM, may be attributed to the lowered binding affinity of the supramolecular species at a low concentration during the sample coatings.

On the other hand, the solution of **1**-AuNP/trisDB24C8 (w/w = 1:2.5) was analyzed by TEM (Figure 7c,d). Both dimers and trimers are observed (Figure 7d; dimer, blue circle; trimer, red circle). Among other solutions with different titration ratios, the TEM images of the solution w/w = 1:2.5 yield higher number of trimers (Figure S17b in Supporting Information). No tetramers or higher order supramolecular structures are observed under TEM (Figure 8b). The apparent spacing between the AuNPs in the trimer structures ranges from 1.5 to 5.1 nm (Figures S21−S23 in Supporting Information). Interestingly, the trimers mostly appear as triangular shapes but with a small amount of near-linear ones. The possibility of forming the novel near-linear trimers may be attributed to the adaptation of a folded trisDB24C8 conformation (Figure S23 in Supporting Information) as well as the aliphatic attractive force between the AuNPs' surfaces offered by numerous *n*-butyl peripheral surface groups (Figure 9).

SUMMARY

For the first time, amine monofunctional gold nanoparticles (**1**-AuNPs) were synthesized and purified in a hydrogen-bonded supramolecular manner using a crown-ether-decorated polystyrene resin and crown-ether-decorated superparamagnetic iron oxide nanoparticles. The purified monofunctional gold nanoparticles were characterized by TEM, IR, XPS, and UV/visible absorption spectroscopies. The pH-switchable, hydrogen-bonded molecular recognition motifs have been proven as versatile templates. By using our ap-

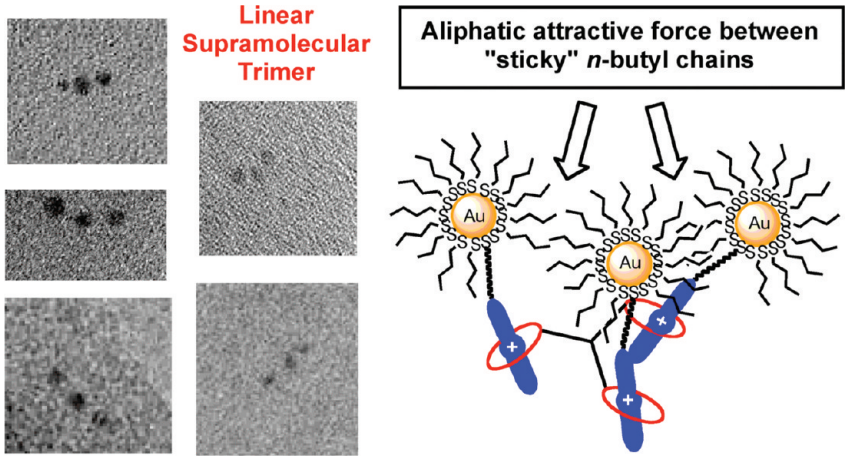

Figure 9. TEM images revealing the near-linear supramolecular trimers and the graphical representation of the formation of near-linear supramolecular trimers by virtue of the aliphatic attractive force between the AuNPs' surfaces offered by the numerous *n*-butyl peripheral surface groups.

proach, the product **1**-AuNPs was obtained in near-quantitative yield, which has been confirmed by a complete shift to form a plasmonic resonance band in the UV/visible absorption spectrum with bisDB24C8 (w/w = 1:1). In addition to the reusability and recyclability of the material systems, the preparation and purification cycles could be repeated numerous times. Chromatographic separation of products is not required.

Formation of the supramolecular dimers and trimers of the monofunctional gold nanoparticles has been observed under TEM and characterized by the distinctive plasmonic absorptions. The strategy presented herein will allow one to control precisely the number of active molecules per nanoparticle, thus offering unprecedented opportunities to more effectively promote different biological and medical applications.[4,5] For instance, by exploiting well-defined 1:1 biomolecule−NP conjugates, it will be possible to study, at a truly molecular scale, the structure and the dynamic organization of the plasma membrane (*i.e.*, by tracking the motion of individual intracellular proteins). Such studies have been so far a major challenge in cell biology.[55] In the same manner, sophisticated nanoparticle−biomolecule hybrid systems, in which the number of biomolecules per nanoparticle is precisely controlled, would allow more accurate detection of molecules associated with particular diseases, offering drastic improvements in disease detection, therapy, and prevention.[1−3,56]

METHODS

PS-DB24C8. To a mixture of DB24C8-CO_2H (0.74 g, 1.51 mmol) in DMF (5 mL) and NEt_3 (0.21 mL, 1.50 mmol) at −3 °C was added IBCF (0.20 mL, 1.54 mmol) to give a pale yellow solution. After 30 min, PS resin (2.13 g, preswollen in DMF (10 mL) for 1 h) and a catalytic amount of DMAP were added to give a pale brown solution with the dispersion of resin. The reaction was stirred overnight at ambient temperature. The resulting solution was filtered and washed with CH_2Cl_2 several times. The filtered resin was obtained as the PS-DB24C8. Furthermore, the excess solvents of the filtrate were evaporated. The resulting solid was redissolved in $CHCl_3$, and the solution was washed with saturated $NaHCO_3$, water, and 2 M HCl. The pH of the solution was carefully adjusted to 4. The organic layer was washed with saturated NaCl, dried (anhydrous $MgSO_4$), and filtered. Then, the filtrate was evaporated to dryness under reduced pressure to give a white solid. The remaining amount of the DB24C8-CO_2H as in the filtrate was determined by ^1H NMR with the addition of known amount of $MeNO_2$ (5.4 μL) as an internal standard. By comparing the integration ratio between the methyl hydrogen signal from the internal standard and the ethylene glycol hydrogen signal from the crown ether, the yield of the reaction was found to be 77%. The PS-DB24C8 was characterized by the presence of the significant C═O absorption band at 1741 cm^{-1} in the FT-IR spectrum (KBr, solid). A control experiment was done with the same procedure, but the solvent was changed to CH_2Cl_2, from which no reaction occurred, that is, 100% of the DB24C8-CO_2H was present in the filtrate.

PS-DB24C8⊃[1 · HPF_6]$_n$. All the resin PS-DB24C8 prepared from the previous step was swelled in CH_2Cl_2 (10.3 mL) and MeCN (1.7 mL) with gentle mechanical shaking. Compound **1** · HPF_6 (0.48 g, 0.82 mmol) was added to the resin suspension at 40 °C for 1 h and at ambient temperature for 2 h. Subsequently, the resin was filtered and washed with CH_2Cl_2 (10 mL): FTIR (KBr, solid) ν = 3231 and 3252 cm^{-1} [N^+H_2], 1735 cm^{-1} [C═O].

PS-DB24C8⊃[1 · HPF_6-AuNP]$_n$. Butanethiolate-coated gold nanoparticles (10.0 mg), as prepared from the modified literature procedure,[14] were added to a solution of PS-DB24C8⊃[**1** · HPF_6]$_n$ in CH_2Cl_2 (10.3 mL) and MeCN (1.7 mL). The mixture was shaken gently at 40 °C for 4 h and at ambient temperature for 24 h. The resulting resin was then filtered and washed with CH_2Cl_2 (10 mL): FTIR (KBr, solid) ν = 3233 cm^{-1} [N^+H_2], 1737 cm^{-1} [C═O]; far-IR (suspension in paraffin oil) ν = 249 cm^{-1} [Au−S].

1-AuNP. The resin PS-DB24C8⊃[**1** · HPF_6-AuNP]$_n$ was suspended in CH_2Cl_2 (10.3 mL) and MeCN (1.7 mL). NEt_3 (0.23 mL) was added to the suspension with gentle mechanical shaking for 40 min at ambient temperature. The resin was then filtered and washed with CH_2Cl_2 (10 mL). The filtrate was evaporated *in vacuo*, and the residue was washed with cold EtOH. Finally, the resulting solid was dissolved in CH_2Cl_2. Purification was facilitated with SPIO−DB24C8: First, a solution of SPIO−DB24C8 (1.0 g) in CH_2Cl_2 (3 mL) was sonicated for 10 min. The crude **1**-AuNP products in CH_2Cl_2 were mixed with the SPIO−DB24C8 solution. H-TFA (0.15 mL, 1.95 mmol) was added to the mixture and shaken mechanically for 15 min. A magnet was placed near the reaction flask to magnetically attract all of the magnetic particles. The supernatant was discarded and placed aside, while the magnetic particles were washed with CH_2Cl_2 under the application of magnetic field. A solution of Et_3N (0.28 mL, 2.00 mmol) in CH_2Cl_2 (5 mL) was added to the resulting magnetic particles. The solution was then mechanically shaked for 15 min. A magnet was placed near the reaction flask to magnetically attract all the magnetic particles, and then the supernatant was collected, washed with H_2O, and dried *in vacuo* to give the purified **1**-AuNPs (6.3 mg): FTIR (KBr, solid) ν = 1733 cm^{-1} [C═O], 804 cm^{-1} [*para*-subsituted aromatic C−H]; far-IR (suspension in paraffin oil) ν = 249 cm^{-1} [Au−S]; UV/visible (CH_2Cl_2, L mg^{-1} cm^{-1}) ε = 2.00, 0.84, λ_{max} = 265.5 and 525 nm. Conversion yields: 3.0 mg of 1-AuNP per gram of PS resin (−OH density = 1.0−1.5

mmol/g) and 2.3 mg of 1-AuNP per gram of PS-DB24C8 (−DB24C8 density ~ 1.0 mmol/g).

General Procedures for the Self-Assembly of Supramolecular Dimers and Trimers. The purified **1**-AuNPs were mixed with different ratios (w/w) of bisDB24C8 and trisDB24C8 in a CH_2Cl_2/H-TFA (22:1) solution to form the bisDB24C8⊃[**1** · HTFA-AuNP]$_2$ and trisDB24C8⊃[**1** · HTFA-AuNP]$_3$, respectively. The concentration of the **1**-AuNP was 0.2 ± 0.05 mg/mL in CH_2Cl_2/H-TFA (22:1). Aliquots of these solutions were used directly for TEM and UV/visible spectroscopic measurements.

Acknowledgment. This work is supported by a Strategic Investments Scheme and a Direct Grant of Research (2060336) administrated by The Chinese University of Hong Kong as well as The Research Grants Council of Hong Kong (CUHK401707). Dr. Ka-Wai Wong and Mr. Man-Hau Yeung are gratefully acknowledged for the help on TEM measurements.

Supporting Information Available: Experimental procedures, analytical and spectral characterization data, molecular modeling, and expanded discussions of peripheral findings and control experiments. This material is available free of charge *via* the Internet at http://pubs.acs.org.

REFERENCES AND NOTES

1. Michalet, X.; Pinaud, F. F.; Bentolila, L. A.; Tsay, J. M.; Doose, S.; Li, J. J.; Sundaresan, G.; Wu, A. M.; Gambhir, S. S.; Weiss, S. Quantum Dots for Live Cells, *In Vivo* Imaging, and Diagnostics. *Science* **2005**, *307*, 538–544.
2. Jain, P. K.; Huang, X. H.; El-Sayed, I. H.; El-Sayed, M. A. Noble Metals on the Nanoscale: Optical and Photothermal Properties and Some Applications in Imaging, Sensing, Biology, and Medicine. *Acc. Chem. Res.* **2008**, *41*, 1578–1586.
3. Huo, Q. A Perspective on Bioconjugated Nanoparticles and Quantum Dots. *Colloids Surf., B* **2007**, *59*, 1–10.
4. Kane, R. S.; Stroock, A. D. Nanobiotechnology: Protein−Nanomaterial Interactions. *Biotechnol. Prog.* **2007**, *23*, 316–319.
5. Grainger, D. W.; Castner, D. G. Nanobiomaterials and Nanocatalysis: Opportunities for Improving the Science to Benefit Biomedical Technologies. *Adv. Mater.* **2008**, *20*, 867–877.
6. Hostetler, M. J.; Templeton, A. C.; Murray, R. W. Dynamics of Place-Exchange Reactions on Monolayer-Protected Gold Cluster Molecules. *Langmuir* **1999**, *15*, 3782–3789.
7. Shenhar, R.; Rotello, V. M. Nanoparticles: Scaffolds and Building Blocks. *Acc. Chem. Res.* **2003**, *36*, 549–561.
8. Daniel, M.-C.; Astruc, D. Gold Nanoparticles: Assembly, Supramolecular Chemistry, Quantum-Size-Related Properties, and Applications toward Biology, Catalysis, and Nanotechnology. *Chem. Rev.* **2004**, *104*, 293–346.
9. Rosi, N. L.; Mirkin, C. A. Nanostructures in Biodiagnostics. *Chem. Rev.* **2005**, *105*, 1547–1562.
10. You, C. C.; Verma, A.; Rotello, V. M. Engineering the Nanoparticle−Biomacromolecule Interface. *Soft Matter* **2006**, *2*, 190–204.
11. Stewart, M. E.; Anderton, C. R.; Thompson, L. B.; Maria, J.; Gray, S. K.; Rogers, J. A.; Nuzzo, R. G. Nanostructured Plasmonic Sensors. *Chem. Rev.* **2008**, *108*, 494–521.
12. Zhao, W.; Brook, M. A.; Li, Y. F. Design of Gold Nanoparticle-Based Colorimetric Biosensing Assays. *ChemBioChem* **2008**, *9*, 2363–2371.
13. Murphy, C. J.; Gole, A. M.; Stone, J. W.; Sisco, P. N.; Alkilany, A. M.; Goldsmith, E. C.; Baxter, S. C. Gold Nanoparticles in Biology: Beyond Toxicity to Cellular Imaging. *Acc. Chem. Res.* **2008**, *41*, 1721–1730.
14. Worden, J. G.; Shaffer, A. W.; Huo, Q. Controlled Functionalization of Gold Nanoparticles through a Solid Phase Synthesis Approach. *Chem. Commun.* **2004**, 518–519.
15. Sung, K.-M.; Mosley, D. W.; Peelle, B. R.; Zhang, S.; Jacobson, J. M. Synthesis of Monofunctionalized Gold Nanoparticles by Fmoc Solid-Phase Reactions. *J. Am. Chem. Soc.* **2004**, *126*, 5064–5065.
16. Krüger, C.; Agarwal, S.; Greiner, A. Stoichiometric Functionalization of Gold Nanoparticles in Solution through a Free Radical Polymerization Approach. *J. Am. Chem. Soc.* **2008**, *130*, 2710–2711.
17. Brousseau, L. C., III; Novak, J. P.; Marinakos, S. M.; Feldheim, D. L. Assembly of Phenylacetylene-Bridged Gold Nanocluster Dimers and Trimers. *Adv. Mater.* **1999**, *11*, 447–449.
18. Deng, Z.; Mao, C. Molecular Lithography with DNA Nanostructures. *Angew. Chem., Int. Ed.* **2004**, *43*, 4068–4070.
19. Huo, F.; Lytton-Jean, A. K. R.; Mirkin, C. A. Asymmetric Functionalization of Nanoparticles Based on Thermally Addressable DNA Interconnects. *Adv. Mater.* **2006**, *18*, 2304–2306.
20. Aldaye, F. A.; Sleiman, H. F. Sequential Self-Assembly of a DNA Hexagon as a Template for the Organization of Gold Nanoparticles. *Angew. Chem., Int. Ed.* **2006**, *45*, 2204–2209.
21. Zheng, J.; Constantinou, P. E.; Micheel, C.; Alivisatos, A. P.; Kiehl, R. A.; Seeman, N. C. Two-Dimensional Nanoparticle Arrays Show the Organization Power of Robust DNA Motifs. *Nano Lett.* **2006**, *6*, 1502–1504.
22. Aldaye, F. A.; Sleiman, H. F. Dynamic DNA Templates for Discrete Gold Nanoparticle Assemblies: Control of Geometry, Modularity, Write/Erase and Structural Switching. *J. Am. Chem. Soc.* **2007**, *129*, 4130–4131.
23. Huo, Q.; Worden, J. G. Monofunctional Gold Nanoparticles: Synthesis and Applications. *J. Nanopart. Res.* **2007**, *9*, 1013–1025.
24. DeVries, G. A.; Brunnbauer, M.; Hu, Y.; Jackson, A. M.; Long, B.; Neltner, B. T.; Uzun, O.; Wunsch, B. H.; Stellacci, F. Divalent Metal Nanoparticles. *Science* **2007**, *315*, 358–361.
25. Claridge, S. A.; Liang, H. W.; Basu, S. R.; Fréchet, J. M. J.; Alivisatos, A. P. Isolation of Discrete Nanoparticle−DNA Conjugates for Plasmonic Applications. *Nano Lett.* **2008**, *8*, 1202–1206.
26. Nykypanchuk, D.; Maye, M. M.; van der Lelie, D.; Gang, O. DNA-Guided Crystallization of Colloidal Nanoparticles. *Nature* **2008**, *451*, 549–552.
27. Park, S. Y.; Lytton-Jean, A. K. R.; Lee, B.; Weigand, S.; Schatz, G. C.; Mirkin, C. A. DNA-Programmable Nanoparticle Crystallization. *Nature* **2008**, *451*, 553–556.
28. Chen, G.; Wang, Y.; Tan, L. H.; Yang, M.; Tan, L. S.; Chen, Y.; Chen, H. High-Purity Separation of Gold Nanoparticle Dimers and Trimers. *J. Am. Chem. Soc.* **2009**, *131*, 4218–4219.
29. Browne, W. R.; Feringa, B. L. Making Molecular Machines Work. *Nat. Nanotechnol.* **2006**, *1*, 25–35.
30. Kay, E. R.; Leigh, D. A.; Zerbetto, F. Synthetic Molecular Motors and Mechanical Machines. *Angew. Chem., Int. Ed.* **2007**, *46*, 72–191.
31. Descalzo, A. B.; Marínez-Máñez, R.; Sancenón, F.; Hoffmann, K.; Rurack, K. The Supramolecular Chemistry of Organic−Inorganic Hybrid Materials. *Angew. Chem., Int. Ed.* **2006**, *45*, 5924–5948.
32. Saha, S.; Leung, K. C.-F.; Nguyen, T. D.; Stoddart, J. F.; Zink, J. I. Nanovalves. *Adv. Funct. Mater.* **2007**, *17*, 685–693.
33. Leung, K. C.-F.; Mendes, P. M.; Magonov, S. N.; Northrop, B. H.; Kim, S.; Patel, K.; Flood, A. H.; Tseng, H.-R.; Stoddart, J. F. Supramolecular Self-Assembly of Dendronized Polymers: Reversible Control of the Polymer Architectures through Acid−Base Reactions. *J. Am. Chem. Soc.* **2006**, *128*, 10707–10715.
34. Leung, K. C.-F.; Chak, C.-P.; Lo, C.-M.; Wong, W.-Y.; Xuan, S. H.; Cheng, C. H. K. pH-Controllable Supramolecular Systems. *Chem. Asian J.* **2009**, *4*, 364–381.
35. Lu, A.-H.; Salabas, E. L.; Schüth, F. Magnetic Nanoparticles: Synthesis, Protection, Functionalization, and Application. *Angew. Chem., Int. Ed.* **2007**, *46*, 1222–1244.
36. Latham, A. H.; Williams, M. E. Controlling Transport and Chemical Functionality of Magnetic Nanoparticles. *Acc. Chem. Res.* **2008**, *41*, 411–420.
37. Kolchinski, A. G.; Busch, D. H.; Alcock, N. W. Gaining Control over Molecular Threading: Benefits of Second Coordination Sites and Aqueous-Organic Interfaces in

Rotaxane Synthesis. *J. Chem. Soc., Chem. Commun.* **1995**, 1289–1291.
38. Ashton, P. R.; Campbell, P. J.; Chrystal, E. J. T.; Glink, P. T.; Menzer, S.; Philp, D.; Spencer, N.; Stoddart, J. F.; Tasker, P. A.; Williams, D. J. Dialkylammonium Ion/Crown Ether Complexes: The Forerunners of a New Family of Interlocked Molecules. *Angew. Chem., Int. Ed.* **1995**, *34*, 1865–1869.
39. Badjic, J. D.; Ronconi, C. M.; Stoddart, J. F.; Balzani, V.; Silvi, S.; Credi, A. Operating Molecular Elevators. *J. Am. Chem. Soc.* **2006**, *128*, 1489–1499.
40. Laurent, S.; Forge, D.; Port, M.; Roch, A.; Robic, C.; Elst, L. V.; Muller, R. N. Magnetic Iron Oxide Nanoparticles: Synthesis, Stabilization, Vertorization, Physiochemical Characterizations, and Biological Applications. *Chem. Rev.* **2008**, *108*, 2064–2110.
41. Yamaguchi, N.; Hamilton, L. M.; Gibson, H. W. Dendritic Pseudorotaxanes. *Angew. Chem., Int. Ed.* **1998**, *37*, 3275–3279.
42. The association constants (K_a) for the 1:1 [DBA⊂DB24C8] pseudorotaxane formation are approximately 10^5-10^6 in CH_2Cl_2 and 10^2-10^3 in MeCN, which were measured using the isothermal titration calorimetry at 298 K. See: South, C. R.; Higley, M. N.; Leung, K. C.-F.; Lanari, D.; Nelson, A.; Grubbs, R. H.; Stoddart, J. F.; Weck, M. Self-Assembly with Block Copolymers through Coordination of SCS-Pd^{II} Pincer Complexes and Pseudorotaxane Formation. *Chem.—Eur. J.* **2006**, *12*, 3789–3797.
43. South, C. R.; Leung, K. C.-F.; Lanari, D.; Stoddart, J. F.; Weck, M. Noncovalent Side-Chain Functionalization of Terpolymers. *Macromolecules* **2006**, *39*, 3738–3744.
44. Leung, K. C.-F.; Nguyen, T. D.; Stoddart, J. F.; Zink, J. I. Supramolecular Nanovalves Controlled by Proton Abstraction and Competitive Binding. *Chem. Mater.* **2006**, *18*, 5919–5928.
45. For the synthesis of SPIO-DB24C8, see Supporting Information.
46. Coates, J. Interpretation of Infrared Spectra, A Practical Approach. In *Encyclopedia of Analytical Chemistry*; Meyers, R. A., Ed.; John Wiley & Sons: Chichester, UK, 2000; pp 10815−10837.
47. Lin, S.-Y.; Tsai, Y.-T.; Chen, C.-C.; Lin, C.-M.; Chen, C.-H. Two-Step Functionalization of Neutral and Positively Charged Thiols onto Citrate-Stabilized Au Nanoparticles. *J. Phys. Chem. B* **2004**, *108*, 2134–2139.
48. Kluth, G. J.; Carraro, C.; Maboudian, R. Direct Observation of Sulfur Dimers in Alkanethiol Self-Assembled Monolayers on Au(111). *Phys. Rev. B* **1999**, *59*, R10449–R10452.
49. Mock, J. J.; Hill, R. T.; Degiron, A.; Zauscher, S.; Chilkoti, A.; Smith, D. R. Distance-Dependent Plasmon Resonant Coupling between a Gold Nanoparticle and Gold Film. *Nano Lett.* **2008**, *8*, 2245–2252.
50. Jiang, P.; Xie, S.-S.; Yao, J.-N.; Pang, S.-J.; Gao, H.-J. The Stability of Self-Organized 1-Nonanethiol-Capped Gold Nanoparticle Monolayer. *J. Phys. D: Appl. Phys.* **2001**, *34*, 2255–2259.
51. Wu, P.; Feldman, A. K.; Nugent, A. K.; Hawker, C. J.; Scheel, A.; Voit, B.; Pyun, J.; Fréchet, J. M. J.; Sharpless, K. B.; Fokin, V. V. Efficiency and Fidelity in a Click-Chemistry Route to Triazole Dendrimers by the Copper(I)-Catalyzed Ligation of Azides and Alkynes. *Angew. Chem., Int. Ed.* **2004**, *43*, 3928–3932.
52. Aprahamian, I.; Miljanic, O. S.; Dichtel, W. R.; Isoda, K.; Yasuda, T.; Kato, T.; Stoddart, J. F. Clicked Mechanically Interlocked Molecules. *Bull. Chem. Soc. Jpn.* **2007**, *80*, 1856–1869.
53. Elghanian, R.; Storhoff, J. J.; Mucic, R. C.; Letsinger, R. L.; Mirkin, C. A. Selective Colorimetric Detection of Polynucleotides Based on the Distance-Dependent Optical Properties of Gold Nanoparticles. *Science* **1997**, *277*, 1078–1081.
54. Templeton, A. C.; Wuelfing, W. P.; Murray, R. W. Monolayer-Protected Cluster Molecules. *Acc. Chem. Res.* **2000**, *33*, 27–36.
55. Jamieson, T.; Bakhshi, R.; Petrova, D.; Pocock, R.; Imani, M.; Seifalian, A. M. Biological Applications of Quantum Dots. *Biomaterials* **2007**, *28*, 4717–4732.
56. Sanvicens, N.; Marco, M. P. Multifunctional Nanoparticles—Properties and Prospects for Their Use in Human Medicine. *Trends Biotechnol.* **2008**, *26*, 425–433.